Petroleum Science 23 (2026) 1053–1065

Contents lists available at ScienceDirect

Petroleum Science

journal homepage: www.keaipublishing.com/en/journals/petroleum-science

Original Paper

Assessment of shale hydrocarbon evaporative loss during exposure: Insights from online low-field nuclear magnetic resonance observations in the Qingshankou Formation, Songliao Basin, China

Xue-Ning Qi [a,b], Hua Tian [a,b], Xiao-Mei Wang [a,b,*], Ming-Hao Wu [a,b], Yu-Ke Liu [a,b], Shui-Chang Zhang [a,b]

[a] Research Institute of Petroleum Exploration and Development, PetroChina, Beijing, 100083, China
[b] Key Laboratory of Petroleum Geochemistry, China National Petroleum Corporation, Beijing, 100083, China

ARTICLE INFO

Article history:
Received 19 January 2025
Received in revised form
9 May 2025
Accepted 11 September 2025
Available online 17 September 2025

Edited by Xi Zhang and Jie Hao

Keywords:
Evaporative hydrocarbon loss
Shale oil
Songliao Basin
Low-field nuclear magnetic resonance
Qingshankou Formation

ABSTRACT

Understanding the evaporative loss of shale oil is critical for the shale oil resources assessment. However, previous studies have largely neglected the rapid evaporative loss of shale oil that occurs immediately after drill cores are retrieved to the surface at the well site. Thus, the factors influencing the evaporative loss of shale oil during thermal evolution remain inadequately explored. In this study, closed-system pyrolysis experiments were carried out to the artificially mature Qingshankou Formation shales. Subsequently, low-field nuclear magnetic resonance (LF-NMR) techniques were utilized to monitor the variations in oil content of the shales under different exposure times. Our experimental approach successfully reconstructed the entire evaporative loss process of shale oil, spanning from its original subsurface location to the well site, from the well site to the laboratory, and ultimately to long-term core storage. We find that the maximum loss of shale oil reaches approximately 10% within the first 10 h following the retrieval of drill cores from the subsurface to the ground, followed by a gradual deceleration, and the maximum loss ranges from 11% to 89%. As thermal maturity increases to a range of R_o = 0.89%–1.20%, the loss proportion of shale oil shows a decreasing trend, which can be attributed to the reduction in total organic carbon (TOC) content. It is worth mentioning that the loss proportion of shale oil exhibits a continuous increasing trend at the thermal range of 1.20%–1.75%. At this stage, the hydrocarbon composition (C_6–C_{14}/C_{15+} ratio) may be the mainly controlling factors for the shale oil loss proportion, while TOC content and nanopore volume serve as secondary factors. Our analyses reveal that hydrocarbon evaporative loss of shale oil is complex and involves various factors, especially the first 10 h during the transfer of the shale from its in-situ reservoir to the surface at the well site, which is critical to the understanding of shale oil occurrence and accurate resource assessment.
© 2025 The Authors. Publishing services by Elsevier B.V. on behalf of KeAi Communications Co. Ltd. This is an open access article under the CC BY license (http://creativecommons.org/licenses/by/4.0/).

1. Introduction

Shale oil is an important global energy resource (Hughes, 2013; Hopkins, 2017; Hong et al., 2025). However, inaccurate estimates of the initial total content of shale oil can lead to erroneous assessments of shale oil resources (Abrams et al., 2017; Wang et al., 2022). Especially, the evaporative hydrocarbon loss of shale oil is often ignored during the evaluation of the total oil content of shale (Jarvie, 2012; Michael et al., 2013; Jiang et al., 2016; Hu et al., 2021; Wang et al., 2022).

Previous studies have investigated evaporative loss of shale oil from the well site to the laboratory or during the storage of core samples at ambient conditions in different regions (Song et al., 2013; Zhu et al., 2015; Jiang et al., 2016; Chen et al., 2017, 2018; Sun, 2020; Zhao et al., 2023). While the previous studies have generally overlooked the evaporative loss of hydrocarbons during drilling and core recovery to the surface at the well site, there might be an enormous loss of hydrocarbons caused by changes in temperature and pressure during this process (Jarvie, 2012).

The studies from the well site to the laboratory or during the storage of core samples have been carried out in different basins,

* Corresponding author.
E-mail address: wxm01@petrochina.com.cn (X.-M. Wang).
Peer review under the responsibility of China University of Petroleum (Beijing).

https://doi.org/10.1016/j.petsci.2025.09.024
1995-8226/© 2025 The Authors. Publishing services by Elsevier B.V. on behalf of KeAi Communications Co. Ltd. This is an open access article under the CC BY license (http://creativecommons.org/licenses/by/4.0/).

For example, in the Bohai Bay Basin in China, the shale oil loss in the Paleogene Shahejie Formation varies in different depressions, with reported losses of 9%–52% of the storage of core samples at ambient conditions in the Jiyang Depression (Song et al., 2013; Chen et al., 2017). The Dongying Depression contains shale with total organic carbon (TOC) contents ranging from 1.4 wt% to 8.7 wt% (mostly 2.0–4.0 wt%; with an average of 3.1 wt%) that underwent shale oil loss of 5.23%–25.65% after 30 days of storage under ambient conditions (Zhu et al., 2015). The Damintun Sag contains shale with TOC contents of 0.47–14.0 wt% (mean = 6.45 wt%) that exhibited shale oil maximum loss proportion of 37.5%–47.4% (Chen et al., 2017). Shale samples from other basins exhibit varying degrees of hydrocarbon loss under ambient conditions. A core sample of organic-rich shale (TOC = 11.90 wt%) from the Devonian Duvernay Formation in the Western Canada Sedimentary Basin stored for 2 years lost 15% of its oil content after 360 h exposed to open air, increasing to 22.5% after 1300 h. An organic-poor shale (TOC = 0.86 wt%) from the Ordovician Lotbinière Formation in the St. Lawrence Platform, Quebec, Canada kept at ambient conditions for 6 months, showed 15% hydrocarbon evaporative loss after 21 h and 29% after 170 h after being exposed to open air (Jiang et al., 2016). In the Junggar Basin, shale samples from the Lucaogou and Fengcheng formations (TOC = 1.03–12.31 wt%, mean = 5.09 wt%) exhibited hydrocarbon losses of 11%–89% after being stored at ambient conditions (Chen et al., 2018). In the Songliao Basin, the hydrocarbon loss was 70% when comparing core samples with those stored under high-pressure conditions (Sun et al., 2020). In the Qaidam Basin, shale from the Ganchaigou Formation experienced hydrocarbon loss of 43% after 43 h of exposure (Zhao et al., 2023). So, the above study focuses on hydrocarbon loss of samples from the well site to the laboratory, the long-term storage of core samples, and sample preparation.

Therefore, we divide the hydrocarbon loss from the recovery of drillcore to final analysis into three stages, stage 1 occurs during the transfer of the shale from its in-situ reservoir to the surface at the well site, which takes about 10 h (Yan et al., 2019). Stage 2 occurs during the transportation of the shale from the well site to the laboratory, which includes core sorting, packaging, and transport. The transportation time depends on the location of the well site (Zhu et al., 2015; Luo et al., 2022), but it is generally ~150 h. Stage 3 occurs during the storage of core samples, with some samples being analyzed promptly, while others are placed in long-term storage (e.g., > 1000 h) until needed (Jiang et al., 2016).

And the previous studies have investigated three key factors controlling shale oil loss: thermal maturity, TOC content, and pore diameter (Song et al., 2013; Zhu et al., 2015; Jiang et al., 2016; Chen et al., 2017, 2018). While they have different opinions about the relationship between thermal maturity (expressed as vitrinite reflectance, R_o) and hydrocarbon loss at different mature stage, during the maturity range of R_o = 0.5%–0.7%, the hydrocarbon loss remains constant (Zhu et al., 2015); the hydrocarbon loss may increase (Song et al., 2013; Zhu et al., 2015) or decrease (Chen et al., 2017, 2018) with increasing maturity at the maturity range of R_o = 0.7%–1.2%; and when over the maturity range of R_o = 1.3%–1.6%, the hydrocarbon loss increases with increasing maturity (Chen et al., 2017, 2018).

The effect of TOC content on shale oil loss is also controversial. Organic-rich shale has a stronger ability to retain oil and gas due to its hydrocarbon adsorption, and thus tends to retain more oil and gas, leading to lower hydrocarbon loss (Jiang et al., 2016; Yan, 2023). However, other studies have suggested that hydrocarbon loss increases at higher TOC contents (Chen et al., 2018). In terms of hydrocarbon composition during evaporative loss, it has been qualitatively observed that lighter components are more prone to hydrocarbon loss than heavier components (Michael et al., 2013; Jarvie et al., 2007; Jiang et al., 2016; Şen and Kozlu, 2020; Sun, 2020).

Some studies have suggested that heavier hydrocarbon components are also susceptible to loss (e.g., Tian et al., 2024). But few studies have quantitatively examined how differences in hydrocarbon composition or carbon numbers affect hydrocarbon loss. Some other studies have highlighted the influence of nanopores during thermal evolution on shale oil loss (Milliken et al., 2013; Zou et al., 2013). When the pore size is below a certain threshold, smaller molecular weight hydrocarbons can be trapped in nanopores (Akkutlu, 2017). An increase in hydrocarbon generation due to the decomposition and transformation of kerogen during hydrocarbon generation leads to an increased nanopore volume (Curtis et al., 2012; Milliken et al., 2013), resulting in more adsorbed hydrocarbons and reduced hydrocarbon loss (Jiang et al., 2016; Chen

obtained for gas chromatography (GC) analysis and the LF-NMR experiments. About 10 g of solid residue was dried in a vacuum oven at 80 °C for 24 h to remove dichloromethane and the dried sample was then subjected to LF-NMR analysis. This study used LF-NMR to continuously monitor the changes in the LF-NMR signal of different shale samples over time, recording the decrease in shale oil content and providing real-time insights into the evaporative loss of hydrocarbons. The experimental process is shown in Fig. 2.

2.2.1. Pyrolysis simulation experiments

The thermal simulation experiments used a water-free closed system to minimize external H contamination. Before the thermal simulation experiments, shale samples (100 g) were dried at 80 °C for 24 h in a vacuum oven to remove moisture. The dried samples were transferred to a stainless-steel tube and sealed with a graphite gasket. The tube was loaded into a high-pressure pyrolysis apparatus developed by the China Petroleum Exploration and Development Research Institute (Mi et al., 2009). A closed system was utilized in this study to replicate subsurface geological conditions. Typically, a 100 g sample was placed in a stainless-steel cylinder (inner diameter: 34 mm), and an axial pressure of 80 MPa was applied from one end of the cylinder to compact the sample.

The burial depth during the simulation was set to 2500 m, with pyrolysis temperatures ranging from 330

The LF-NMR analyses were conducted with a MacroMR12-110H-G system (Niumag, China), with a magnetic field strength of

under low magnetic field to characterize unconventional shale oil and gas, including the shale fluid content, pore size distribution, and fluid occurrence state (Yao and Liu, 2012; Yao et al., 2014; Zhang et al., 2017; Li et al., 2019a; Song and Kausik, 2019; Bai et al., 2023; Zhao et al., 2023; Tian et al., 2024). Since NMR is sensitive to hydrogen-bearing fluids in porous media (Bloembergen et al., 1948; Coates et al., 1999; Meng et al., 2024), its direct measurement of shale oil content provides a more accurate determination of initial shale oil content (Gao and Li, 2015; Zhang et al., 2018; Song and Kausik, 2019; Bai et al., 2023; Meng et al., 2023). The previous studies have suggested the LF-NMR signal is affected by TOC content and clay minerals in the shale (Kausik et al., 2016; Li et al., 2019a). However, in this study, by comparing the LF-NMR signal intensity of the shale samples before and after extraction (Fig. 4), it was observed that the LF-NMR signal of the solid residue after extraction was nearly zero. This indicates the LF-NMR T_2 spectrum exclusively detects signals from hydrocarbons, with negligible interference from solid matrix components.

The normalized LF-NMR signal amplitude (expressed in a.u./g) of shales with

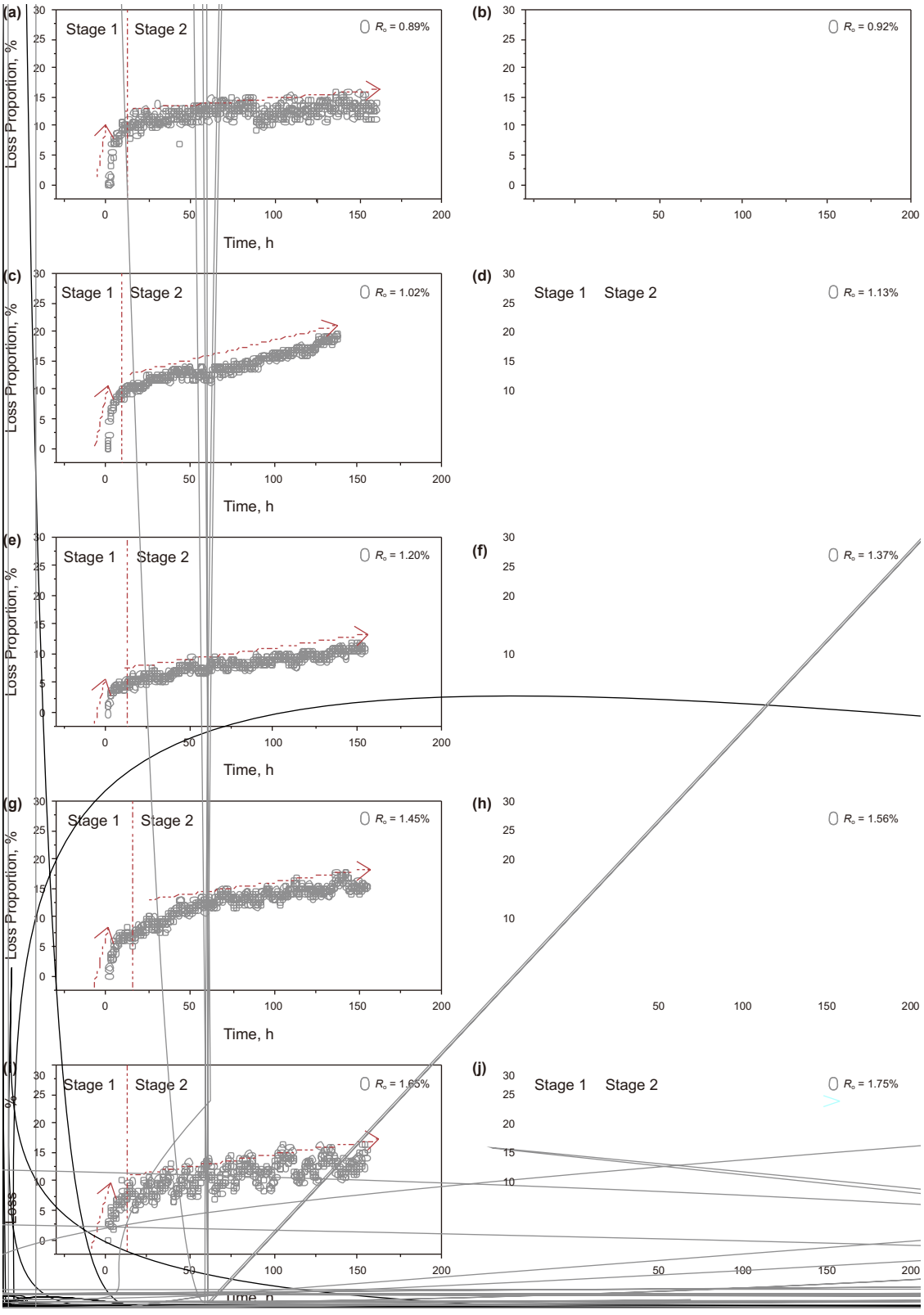

Fig. 6. Proportion of shale oil loss from the Qingshankou Formation shale samples with varying exposure times.

205–311 a.u./g. Within the early oil window (R_o = 1.02%–1.20%), shales exhibited the highest LF-NMR signal amplitudes (515–590 a.u./g), corresponding to peak oil generation observed across the thermal maturity range in this study. After > 1000 h of exposure in open air, the amplitudes decreased to 441, 436, and 416 a.u./g, respectively. Within the R_o = 1.37%–1.56%, Shale samples exhibited the first LF-NMR signal amplitudes were 384, 360, and 323 a.u./g, respectively. Prolonged atmospheric exposure (> 1000 h) induced signal attenuation, with amplitudes declining to 311, 304, and 268 a.u./g, respectively. For overmature shale samples (R_o = 1.65% and

shale oil can b

1.75%), the first LF-NMR signal amplitudes were 210 and 234 a.u./g, respectively. After > 1000 h of exposure under ambient conditions, the amplitudes d eased to 161 and 147 a.u./g, respectively.

Eq. (1) was used to calculate the proportion of shale oil loss at different exposure times (Fig. 7). The evaporative loss of

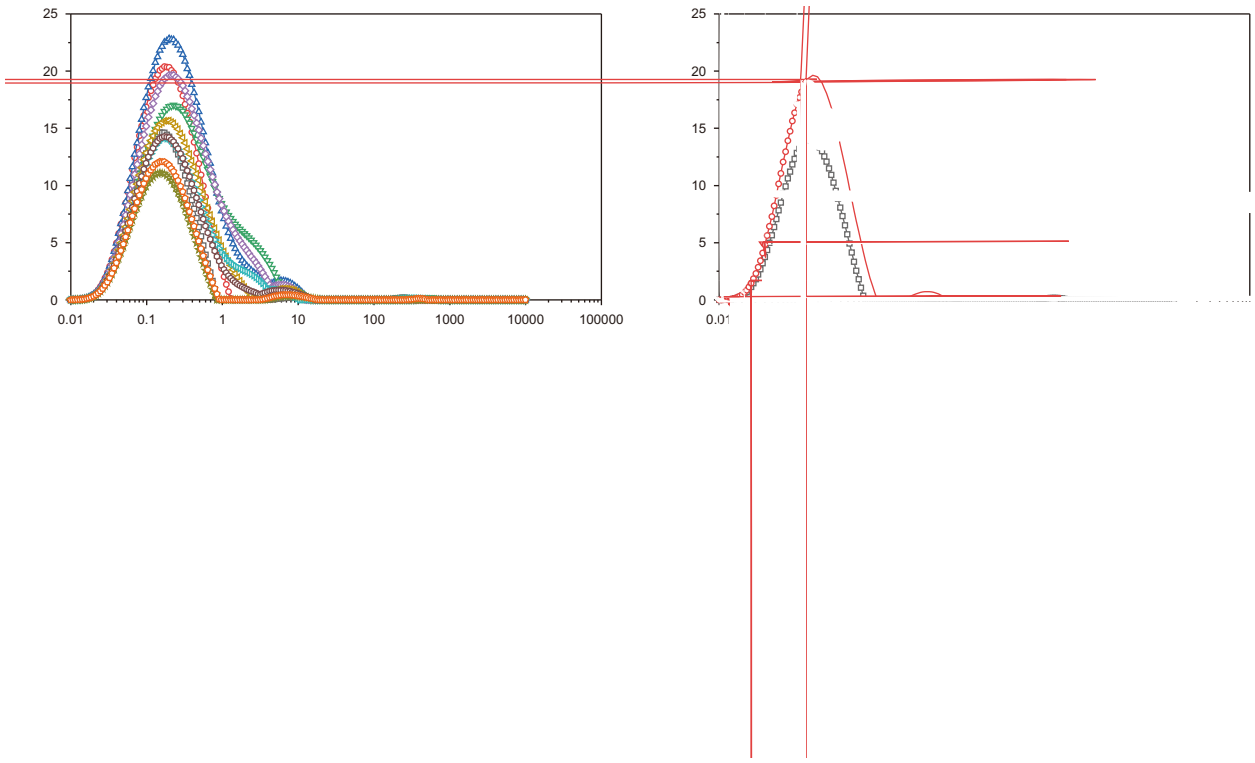

Fig. 9. LF-NMR signal amplitude per gram of rock for the Qingshankou Formation shale samples with increasing maturity at different exposure times. (**a**) 40 min; (**b**) 10 h; (**c**) 150 h; (**d**) > 1000 h.

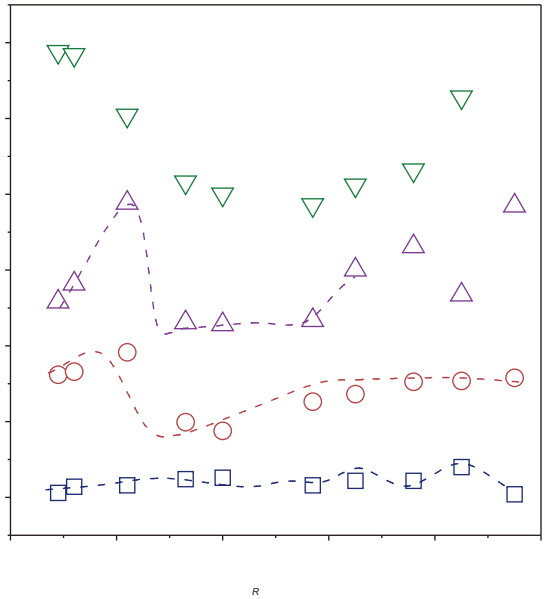

Fig. 10. Relationship between shale oil loss of the Qingshankou Formation shale samples, R_o values (thermal maturity), and exposure time. (**a**) R_o (%) vs. Loss proportion (%/g rock); (**b**) R_o (%) vs. Loss proportion (normalized TOC).

3.3. Factors controlling the evaporative loss of shale oil during thermal evolution

The LF-NMR T_2 spectra of the Qingshankou Formation shale samples (per gram of rock) exhibit progressive shifts under varying exposure durations, indicating dynamic equilibration of hydrocarbon loss processes with thermal evolution (Fig. 9). After reaching equilibrium, the shale oil loss initially decreases and then increases with maturity (Fig. 10(a)). At the initial state (exposure time $\leq$ 40 min), the shale oil loss is not significantly related to the degree of thermal evolution. As exposure time reaches *ca.* 10 h, the proportion of loss is in a dynamic loss state. After an exposure time of > 1000 h, the proportion of loss stabilizes and, as the thermal maturity increases from R_o = 0.89%–1.20%, the proportion of loss

decreases from 29.4% to 20.0%. However, as the maturity increases from R_o = 1.20%–1.75%, the shale oil loss increases from 20.0% to 31.1%, with a minimum loss at R_o = 1.20% (Fig. 10(a)).

Shale oil evaporative loss during thermal evolution is governed by three key factors: TOC, hydrocarbon composition, and pore size. By comparing the proportion of shale oil loss per unit rock weight and normalized to TOC content, we found that as the TOC content increases, the loss also increases (Fig. 10(a) and (b)). The effect of TOC on shale oil loss depends on the adsorption capacity of the shale samples, as well as the proportion of free oil. The hydrocarbon adsorption capacity per unit TOC mass is constant, implying that higher oil adsorption by the TOC results in greater saturation, making the hydrocarbons more prone to evaporation. For samples with very low oil saturation, if the TOC is in an undersaturated adsorption state, a high TOC content may reduce the shale oil loss (Jiang et al., 2016). Under favorable geological conditions for shale oil exploration and development, TOC content is in a saturated adsorption state with abundant free hydrocarbons. As the TOC content increases, the amount of free oil in the shale also increases

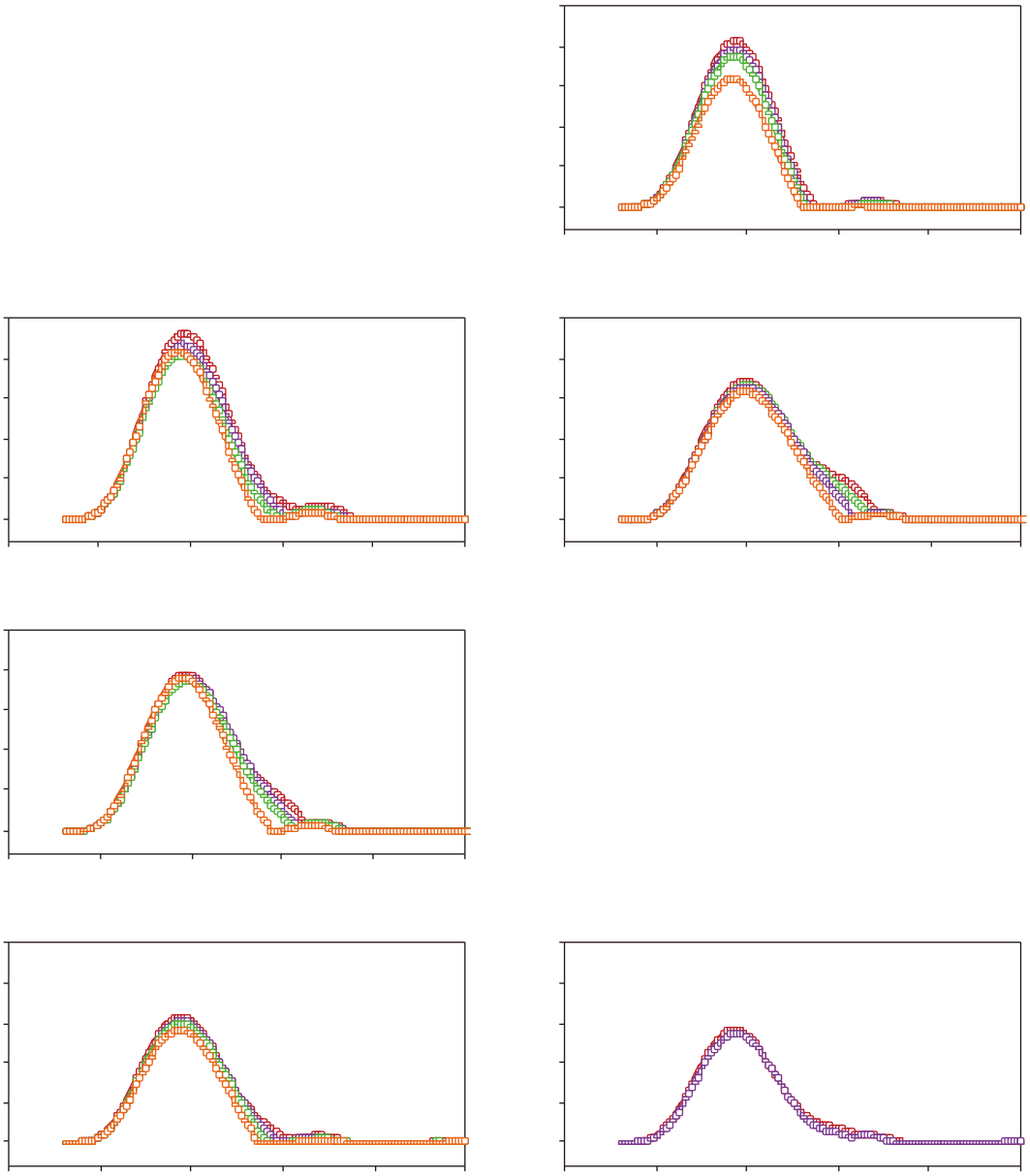

Fig. 13. Changes in oil-bearing pore diameter with exposure time for the Qingshankou Formation shale samples with different maturities.

exposure ($\leq$ 10 h), both the light (C_6–C_{14}) and heavy (C_{15+}) components undergo evaporative loss, driving maximal loss rates in stage 1. With prolonged exposure, depletion of light hydrocarbon fractions shifts mass transfer dominance to heavier components, whose lower evaporative loss kinetics, resulting in rate reductions during stages 2–3 compared to stages 1.

The analyzed shale samples exhibit a nanopore architecture dominated by small oil-bearing pores, as characterized by the LF-

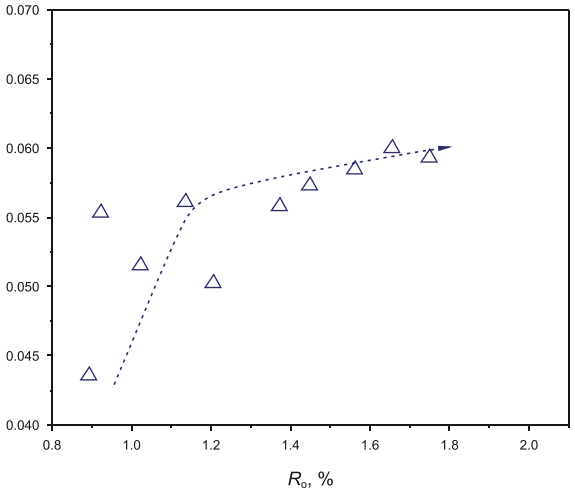

Fig. 14. Relationship between pore volume and shale oil loss for the Qingshankou Formation shale samples.

NMR T_2 spectra. Comparing T_2 relaxation-derived pore diameters (d_{T2}) with the N_2 adsorption data (d_{N2}), yielded an optimal scaling coefficient $C = 40$ for NMR-to-pore size conversion (Fig. 12(a)). A distinct peak and trough occur around the T_2 cutoff value of 2 ms, which effectively divide the entire spectrum into leading and trailing peaks (Fig. 12(b)). The pore diameter range for the leading peak is 0.4–80 nm, and for the trailing peak is 80–1000 nm. Based on the International Union of Pure and Applied Chemistry (IUPAC) classification, nanopores are divided into micropores (pore diameter < 2 nm), mesopores (pore diameter = 2–50 nm), and macropores (pore diameter > 50 nm) (Sing, 1985). The leading peak represents mesopores, while the trailing peak represents macropores.

The LF-NMR T_2 spectra of the shale samples vary with exposure time, revealing differential hydrocarbon evaporative loss with variable pore diameters (Fig. 13). Macropores exhibit rapid hydrocarbon losses, whereas mesopores dominate cumulative loss proportion despite slower loss rates. Following prolonged exposure (> 1000 h), T_2 spectra of the different thermal maturity samples display almost no amplitude signal beyond 2 ms

Table 4
Correlations between TOC content, pore volume, C_6–C_{14}/C_{15+} ratio, and shale oil loss at different maturities.

		Loss proportion (per rock)	
		R_o 0.89%–1.20%	R_o 1.20%–1.75%
TOC	Pearson correlation	0.957[a]	−0.267
	significant (2 tailed)	0.011	0.562
Pore volume	Pearson correlation	−0.289	0.005
	significant (2 tailed)	0.637	0.992
C_6–C_{14}/C_{15+}	Pearson correlation	0.053	0.851[a]
	significant (2 tailed)	0.933	0.015

[a] = Correlation is significant at the 0.05 level (two-tailed distribution).

Fig. 15. Model of the factors that affect shale oil loss.

(Fig. 12(b)), indicating the hydrocarbons in macropores have been completely lost. In contrast, the amplitude signal from the small pores decreases more significantly with exposure time, and the absolute loss from the mesopores increases with exposure time. Zhao et al. (2023) quantified the shale oil loss of the Paleogene Ganchaigou Formation in the Qaidam Basin employing an analogous LF-NMR T_2 spectral analysis technique. After 43 h of pressurized coring, the shale oil loss was 43%, which closely aligned with Stage 2 losses in this study. The LF-NMR T_2 spectrum signal of the Ganchaigou Formation shales ranged from 2 to 10 ms, and significantly longer than those of the studied shale samples. Therefore, the hydrocarbons in large pores were preferentially lost, which explains why the shale oil loss from the Ganchaigou Formation exceeds that in the second stage of the present study.

Organic matter generates organic-hosted nanopores during hydrocarbon generation during the thermal maturity (R_o = 0.89%–1.75%) (Curtis et al., 2012; Wang et al., 2024), with total pore volume increasing from 0.04 to 0.06 cm^3/g (Fig. 14). The increase in nanopores enhanced the shale oil adsorption, resulting in a decrease in shale oil loss. From R_o = 0.89%–1.20%, the nanopores grew rapidly, reducing shale oil loss. However, from R_o = 1.20%–1.75%, the nanopore shows little significant change. This result contradicts the previous assumptions that an increase in nanopores leads to a constant decrease in shale oil loss (Jiang et al., 2016; Chen et al., 2018).

Based on our findings, we developed a comprehensive model identifying the key controls for shale oil loss (Fig. 15). During the low to medium maturity stages (R_o = 0.89%–1.20%), the shale oil loss decreases with increasing maturity, which is due primarily to the decrease in TOC content. The correlations between shale oil loss, TOC content, hydrocarbon composition, and pore volume indicate that TOC content has the strongest correlation with shale oil loss (Table 4). An increase in pore volume contributes to a decrease in the shale oil loss. Previous studies attributed the decrease in shale oil loss to the increasing density of shale oil at greater burial depths in the low to medium maturity stages (Chen et al., 2018). However, the present study used shale samples from laboratory thermal simulation, which effectively eliminates the effect of shale heterogeneity on shale oil loss. Therefore, the shale oil loss in these maturity stages is affected primarily by TOC content, with the hydrocarbon composition and pore volume acting as secondary factors.

In the medium to high maturity stages (R_o = 1.20%–1.75%), the shale oil loss increases with maturity, driven primarily by an increase in the C_6–C_{14}/C_{15+} ratio of the hydrocarbons (Table 4); the changes in pore volume and TOC content are less important.

4. Conclusions and indication

Through the thermal simulation experiments on low-maturity shale samples from the Qingshankou Formation in the Songliao Basin, we obtained the T_2 spectra variation of the shale samples, and quantified both the temporal proportion and rate of shale oil loss with maturities ranging from 0.89% to 1.75% using LF-NMR. The temporal evolution trends and controlling factors of shale oil loss were systematically investigated. The main conclusions are as follows:

The TOC content, hydrocarbon C_6–C_{14}/C_{15+} ratios, and shale oil loss exhibit significant variations across thermal evolution stages. With increasing thermal maturity (R_o = 0.89%–1.75%), the TOC content of the shales decreases from 3.20% to 1.86%. The hydrocarbon C_6–C_{14}/C_{15+} ratios remained stable during early maturation (R_o = 0.89%–1.20%), whereas beyond the peak of hydrocarbon generation (R_o > 1.20%), it increased rapidly from 0.29% to 3.75%.The shale oil loss decreases with increasing maturity at the low to medium maturity stages (R_o = 0.89%–1.20%), and this decrease in shale oil loss is due to the decrease in TOC contents, not the previous results of shale oil density increasing. While the shale oil loss increases with maturity at the medium to high maturity stages (R_o = 1.20%–1.75%), the hydrocarbon composition changing (i.e., an increase in C_6–C_{14}/C_{15+} ratios), is the main factor that causes the increase in shale oil loss rather than TOC content.

Based on the variations in the proportion and rate of shale oil loss for the different shales and exposure times, the evaporative loss of shale oil can be divided into three stages, stage 1 involves a shale oil loss of 0–10.9% (during the first 10 h after core recovery to the surface at the well site), stage 2 involves a shale oil loss of 8.0%–25.0%, and stage 3 involves a shale oil loss of 19.5%–31.1%. So, with increasing exposure time of the shale samples, the shale oil content of the different thermal maturity samples decreased continuously.

The highest proportion of shale oil loss occurred shortly after drilling (< 10 h), reaching approximately 10% of total oil content. Delayed analysis of shale samples after drilling may lead to significant evaporative loss, with maximum proportion of losses ranging from 11% to 89%. The proportion of shale oil loss is different during the following three stages, the first 10 h during the transfer of the shale from its in-situ reservoir to the surface at the well site, the second 150 h of transportation of the shale from the well site to the laboratory, including sorting, packaging, and transport, and last more than 1000 h of storage of samples. Therefore, we should pay more attention to this hydrocarbon evaporative loss at different stages in future shale oil resource assessments.

CRediT authorship contribution statement

Xue-Ning Qi: Methodology, Investigation, Writing – original draft, Conceptualization, Writing – review & editing. **Hua Tian:** Funding acquisition, Writing – review & editing, Methodology. **Xiao-Mei Wang:** Supervision, Funding acquisition, Writing – review & editing. **Ming-Hao Wu:** Writing – original draft. **Yu-Ke Liu:** Visualization. **Shui-Chang Zhang:** Writing – review & editing, Resources.

Declaration of competing interest

The authors declare that they have no known competing financial interests or personal relationships that could have appeared to influence the work reported in this paper.

Acknowledgements

This work was supported by the National Natural Science Foundation of China (Grants U22B6004) and PetroChina R&D Program (Grants 2021DJ0104, 2022-KFKT-09).

References

Abrams, M.A., Gong, C., Garnier, C., et al., 2017. A new thermal extraction protocol to evaluate liquid rich unconventional oil in place and in-situ fluid chemistry. Mar. Petrol. Geol. 88, 659–675. https://doi.org/10.1016/j.marpetgeo.2017.09.014.

Akkutlu, I.Y., 2017. Shale resource assessment in presence of nanopore confinement. In: Proceedings of the 5th Unconventional Resources Technology Conference. American Association of Petroleum Geologists, Austin, Texas, USA. https://doi.org/10.15530/URTEC-2017-2670808.

Bai, L.H., Liu, B., Fu, X.F., et al., 2023. A new method for evaluating the oil mobility based on the relationship between pore structure and state of oil. Geosci. Front. 14, 101684. https://doi.org/10.1016/j.gsf.2023.101684.

Barrett, E.P., Joyner, L.G., Halenda, P.P., 1951. The determination of pore volume and area distributions in porous substances. I. Computations from nitrogen isotherms. J. Am. Chem. Soc. 73, 373–380. https://doi.org/10.1021/ja01145a126.

Bloembergen, N., Purcell, E.M., Pound, R.V., 1948. Relaxation effects in nuclear magnetic resonance absorption. Phys. Rev. 73 (7), 679. https://doi.org/10.1103/PhysRev.73.679.
Chen, G.H., Lu, S.F., Zhang, J.F., et al., 2017. Estimation of enriched shale oil resource potential in E_2s_4L of Damintun sag in Bohai Bay Basin, China. Energy Fuel. 31, 3635–3642. https://doi.org/10.1021/acs.energyfuels.6b03201.
Chen, J.Q., Pang, X.Q., Pang, H., et al., 2018. Hydrocarbon evaporative loss evaluation of lacustrine shale oil based on mass balance method: Permian Lucaogou Formation in Jimusaer Depression, Junggar Basin. Mar. Petrol. Geol. 91, 422–431. https://doi.org/10.1016/j.marpetgeo.2018.01.021.
Clarkson, C.R., Solano, N., Bustin, R.M., et al., 2013. Pore structure characterization of North American shale gas reservoirs using USANS/SANS, gas adsorption, and mercury intrusion. Fuel 103, 606–616. https://doi.org/10.1016/j.fuel.2012.06.119.
Coates, G.R., Xiao, L., Prammer, M.G., 1999. NMR Logging: Principles and Applications. Halliburton Energy Services, Houston, Tex.
Curtis, M.E., Cardott, B.J., Sondergeld, C.H., et al., 2012. Development of organic porosity in the Woodford Shale with increasing thermal maturity. Int. J. Coal Geol. 103, 26–31. https://doi.org/10.1016/j.coal.2012.08.004.
Gao, H., Li, H.Z., 2015. Determination of movable fluid percentage and movable fluid porosity in ultra-low permeability sandstone using nuclear magnetic resonance (NMR) technique. J. Pet. Sci. Eng. 133, 258–267. https://doi.org/10.1016/j.petrol.2015.06.017.
Hong, Z.Q., Meng, M.M., Deng, K., et al., 2025. A quick method for appraising pore connectivity and ultimate imbibed porosity in shale reservoirs. J. Mar. Sci. Eng. 13 (1), 174. https://doi.org/10.3390/jmse13010174.
Hopkins, A.S., 2017. The next energy economy. Science 356, 709. https://doi.org/10.1126/science.aam8696.
Hu, T., Pang, X.Q., Jiang, F.J., et al., 2021. Movable oil content evaluation of lacustrine organic-rich shales: Methods and a novel quantitative evaluation model. Earth Sci. Rev. 214, 103545. https://doi.org/10.1016/j.earscirev.2021.103545.
Hughes, J.D., 2013. A reality check on the shale revolution. Nature 494, 307–308. https://doi.org/10.1038/288688a0.
Jarvie, D.M., 2012. Shale resource systems for oil and gas: Part 2—Shale-oil resource systems shale reservoirs—giant resources for the 21st century. Amer Ass Pet. Geolo. Tulsa, 89–119.
Jarvie, D.M., Hill, R.J., Ruble, T.E., et al., 2007. Unconventional shale-gas systems: the Mississippian barnett shale of north-central Texas as one model for thermogenic shale-gas assessment. AAPG Bull. 91, 475–499. https://doi.org/10.1306/12190606068.
Jiang, C.J., Chen, Z.H., Mort, A., et al., 2016. Hydrocarbon evaporative loss from shale core samples as revealed by Rock-Eval and thermal desorption-gas chromatography analysis: Its geochemical and geological implications. Mar. Petrol. Geol. 70, 294–303. https://doi.org/10.1016/j.marpetgeo.2015.11.021.
Kausik, R., Fellah, K., Feng, L., et al., 2016. High- and low-field NMR relaxometry and diffusometry of the bakken petroleum system. SPWLA. https://go.exlibris.link/vlxZKs9.
Li, J.B., Lu, S.F., Jiang, C.Q., et al., 2019a. Characterization of shale pore size distribution by NMR considering the influence of shale skeleton signals. Energy Fuel. 33, 6361–6372. https://doi.org/10.1021/acs.energyfuels.9b01317.
Li, M.W., Chen, Z.H., Ma, X.X., et al., 2019b. Shale oil resource potential and oil mobility characteristics of the Eocene-Oligocene Shahejie Formation, Jiyang Super-Depression, Bohai Bay Basin of China. Int. J. Coal Geol. 204, 130–143. https://doi.org/10.1016/j.coal.2019.01.013.
Lu, S.F., H, W.B., C, F.W., et al., 2012. Classification and evaluation criteria of shale oil and gas resources: Discussion and application. Petrol. Explor. Dev. 39 (2), 268–276. https://doi.org/10.1016/S1876-3804(12)60042-1.
Luo, C., Zhang, H.X., Zhang, J.Z., et al., 2022. Evaluation of oil content in shale by sealed thermal desorption: A case study of Jurassic Da'an Zhai Member, Sichuan Basin. Pet. Geolo. Exp. 44, 712–718 (in Chinese). https://doi.org/10.11781/sysydz20224712.
Matteson, A., Tomanic, J.P., Herron, M.M., et al., 2000. NMR relaxation of clay/brine mixtures. SPE Reservoir Eval. Eng. 3 (5), 408–413. https://doi.org/10.2118/66185-PA.
Meng, M.M., Hu, Q.H., Wang, Q.Y., et al., 2024. Effect of initial water saturation and water film on imbibition behavior in tight reservoirs using nuclear magnetic resonance technique. Phys. Fluids 36 (5), 056603. https://doi.org/10.1063/5.0209910.
Meng, M.M., Zhang, Y.X., Yuan, B., et al., 2023. Imbibition behavior of oil-saturated rock: Implications for enhanced oil recovery in unconventional reservoirs. Energy Fuel. 37 (18), 13759–13768. https://doi.org/10.1021/acs.energyfuels.3c02501.
Mi, J.K., Zhang, S.C., Wang, X.M., et al., 2009. Comparison of different hydrocarbon generation simulation approaches and key technique. Pet. Geol. Exp. 31, 409–414 (in Chinese). https://doi.org/10.11781/sysydz200904409.
Michael, G.E., Packwood, J., Holba, A., 2013. Determination of in-situ hydrocarbon volumes in liquid rich shale plays. In: SPE/AAPG/SEG unconventional resources technology conference. https:doi.org/168695/URTeC1573030.
Milliken, K.L., Rudnicki, M., Awwiller, D.N., et al., 2013. Organic matter-hosted pore system, Marcellus Formation (Devonian), Pennsylvania. AAPG Bull. 97, 177–200. https://doi.org/10.1306/07231212048.
Şen, Ş., Kozlu, H., 2020. Impact of maturity on producible shale oil volumes in the Silurian (Llandovery) hot shales of the northern Arabian plate, southeastern Turkey. AAPG Bull. 104 (3), 507–524. https://doi.org/10.1306/05141917201.
Sing, K.S., 1985. Reporting physisorption data for gas/solid systems with special reference to the determination of surface area and porosity. Pure Appl. Chem. 57, 603–619. https://doi.org/10.1351/pac198557040603.
Song, G.Q., Lu, S.F., Xu, X.Y., et al., 2013. Resource evaluation method for shale oil and its application. Earth Sci. Front. 20, 221–228 (in Chinese).
Song, Y.Q., Kausik, R., 2019. NMR application in unconventional shale reservoirs—A new porous media research frontier. Prog. Nucl. Magn. Reson. Spectrosc. 112–113, 17–33. https://doi.org/10.1016/j.pnmrs.2019.03.002.
Sun, L.D., 2020. Gulong shale oil (preface). Pet. Geol. Oilfield Dev Daqing 39 (3), 1